The density difference between tissue and neural probes is a key factor for glial scarring.

Lind, Gustav; Eriksson Linsmeier, Cecilia; Schouenborg, Jens

Published in:
Scientific Reports

DOI:
10.1038/srep02942

2013

SCIENTIFIC REPORTS

OPEN

SUBJECT AREAS:
GLIAL BIOLOGY
NEUROSCIENCE

Received
10 May 2013

Accepted
27 September 2013

Published
15 October 2013

Correspondence and requests for materials should be addressed to G.L. (gustav.lind@med.lu.se)

The density difference between tissue and neural probes is a key factor for glial scarring

Gustav Lind, Cecilia Eriksson Linsmeier & Jens Schouenborg

Neuronano Research Center, Department of Experimental Medical Sciences, Medical Faculty, Lund University.

A key to successful chronic neural interfacing is to achieve minimal glial scarring surrounding the implants, as the astrocytes and microglia may functionally insulate the interface. A possible explanation for the development of these reactions is mechanical forces arising between the implants and the brain. Here, we show that the difference between the density of neural probes and that of the tissue, and the resulting inertial forces, are key factors for the development of the glial scar. Two probes of similar size, shape, surface structure and elastic modulus but differing greatly in density were implanted into the rat brain. After six weeks, significantly lower astrocytic and microglial reactions were found surrounding the low-density probes, approaching no reaction at all. This provides a major key to design fully biocompatible neural interfaces and a new platform for *in vivo* assays of tissue reactions to probes with differing materials, surface structures, and shapes.

The implantation of neural interfaces for long periods of time is rapidly becoming an invaluable tool in neuroscience research[1,2]. However, the electrode implants that are used for research today are far from perfect, for example their recording capabilities usually deteriorate over time[3–5]. These shortcomings thus preclude the possibility of conducting long-term studies of for instance the changes in activity in a circuit during the learning of a behaviour. The reason for this is still largely unknown but a major hypothesis is that the glial scar, constituted primarily by astrocytes and microglia, encapsulates the electrodes, functionally insulating the recording surfaces[6–9]. Other reasons for electrode failure can be breakage of electrode leads caused by mechanical stress, local neural degeneration and reorganization of neural circuits intended to be studied[10–12]. However, data from such studies are variable, in many cases there are large numbers of neurons within reasonable recording distance in spite of the inability to record neuronal activity. Therefore, it is of great value to identify the properties of the implanted probes that trigger long-term tissue reactions and reorganization of the nervous tissue, and to find ways to minimize them.

A common hypothesis is that micromotions or rather microforces, between the implanted probe and the tissue cause small injuries that constantly maintain an inflammatory process[3,13]. Such microforces can occur if a rigid electrode is tethered to the skull because of the relative movements between the brain and the skull[13]. In line with this theory, completely untethered implants have been shown to result in significantly smaller long-term scars than tethered ones[14–16]. However, even untethered electrodes leave a substantial astrocytic scar. Considering that microelectrodes are usually made of conductive materials that have higher density than that of the tissue, for example platinum, it is conceivable that microforces that arise due differences in inertia when the animal moves can contribute to the above mentioned tissue reactions.

The aim of this study was to examine the effect of the density of implanted neural probes on the ensuing tissue reactions. To this end, we compared the reactions to two different probes that were implanted in the rat brain, in identical fashion, without any attachment to the skull to alleviate the effect of relative movements between the brain and the skull, which would completely confound the effect of density. The probes had highly similar size, shape, surface structure, and elastic modulus, but differed in density by more than one order of magnitude. The ensuing tissue reactions were evaluated via immunohistochemistry for glial fibrillary acidic protein (GFAP, staining astrocytes), CD68 (ED1, staining microglia) and neuronal nuclei (NeuN). We stained both tissue sections and the explanted probes themselves. With this study design, we intend to isolate the effect of density on the tissue reactions and to provide a full picture of the glial scar, looking at both its' astrocytic and microglial aspects, controlled for any tissue sticking to the probes during explantation. Since microglia and astrocytes are known to affect the electrical properties of implanted cortical electrodes[7,9,17] we consider these markers useful indicators of

biocompatibility (defined as the potential to function integrated with the tissue[18]) of neural implants. We found significantly smaller glial scars surrounding the low-density probes, in some cases approaching no scar at all. This provides strong evidence that the forces resulting from differences in inertia during daily life are sufficient to elicit a substantial glial reaction.

Results

Implants. Two different custom designed probes were used for implantation in this study. Both are needle shaped, 500 μm in diameter, 3.5 mm in length (Fig. 1a) and coated by a 3 μm thick layer of parylene C (Fig. 1b–c). The implants are designed to specifically test the effect of probe density on the ensuing tissue reactions and to preclude any confounding factors such as the effect of the underlying material on the tissue reactions. The first type of probe was made from solid pure platinum, referred to as high-density (HD) probes (Fig. 1a–b), and the second type of probe was made from hollow carbon fibre needles, referred to as low-density (LD) probes (Fig 1a,c). Twelve HD probes and eleven LD probes were included in the final analyses. The density of the HD probe is very close to that of pure platinum (21.45 g/cm^3) while we measured the LD probes densities to be between 1.16–1.48 g/cm^3 (mean 1.35, SD 0.12).

GFAP/ED1 staining of tissue sections. The general tissue reactions to the high-density (HD) probes were qualitatively fully comparable to the tissue reactions observed in our previous studies, as well as to those reported by other laboratories[14,16,19–21]. In brief, we found a dense astrocytic scar of about 10–20 μm encapsulating the probes diminishing further away from the wound, and a relatively sparse distribution of microglia confined to the immediate vicinity of the probes (Fig. 2d–f). However, the low-density (LD) probes generally left an astrocytic scar that is much smaller than that caused by any type of electrode of the same size range examined in similar studies[16,20] (Fig. 2a–c). In fact, several areas surrounding the LD probes were completely devoid of astrocytes (Fig. 2j). Representative images and mean GFAP intensity profile for the two probe types are shown in Fig. 2g. The LD probes exhibited a much lower intensity along the entire intensity profile lines. Comparisons were made between the area under curve in the 0–50 μm and the 50–100 μm regions of the intensity lines for high- and low-density probes. In both areas, the LD probe produced a significantly smaller astrocytic scar than did the HD probe ($P = 0.001$ for 0–50 μm, and $P = 0.0019$ for50–100 μm, Fig. 2g). There were no significant differences between the probes regarding ED1 staining of the tissue ($P = 0.81$, Fig. 2h).

Imaging of explanted probes. It should be noted that the histological analysis above was made after removal of the probes. Therefore, to test whether the difference in tissue reactions observed between LD and HD probes was a true difference, we also quantified the amount of immunoreactivity of GFAP and ED1 present on the explanted probes. Representative images are shown in Fig. 3a–f, as well as a scanning electrode microscopy image of a microglial cell attaching to the surface of a platinum probe (Fig. 3i). There was no significant difference between GFAP intensities ($P = 0.16$, Fig. 3g), indicating that the difference in GFAP reactivity between tissue sections is not an effect of more astrocytes sticking to the LD probes during explantation but most likely a true difference. However, the HD probes had a significantly higher mean ED1 intensity than did the LD probes ($P = 0.0019$, Fig. 3h). Thus, even if the tissue sections showed no differences regarding ED1 reactivity, there still seems to be a true difference between the amounts of microglial cells surrounding the probes *in vivo*. The background fluorescence for each type of probe was tested prior to implantation as a control. Both implants had identical mean intensities.

NeuN staining. We found NeuN-positive cells in very close vicinity, within 5–10 μm, of both probe types in every animal (see Fig. 4d for examples). In some animals however, patches close to both types of implants with lower neuronal density were also observed. Representative images and quantified neuronal densities are shown in Fig. 4a–c. We found no differences between the two probe types regarding neural density ($P = 0.30$, tested in the 0–50 μm ROI).

Discussion

In this study, we explored for the first time the importance of probe density on ensuing long-term tissue reactions. To this end, we constructed implantable probes that were as similar as possible in every

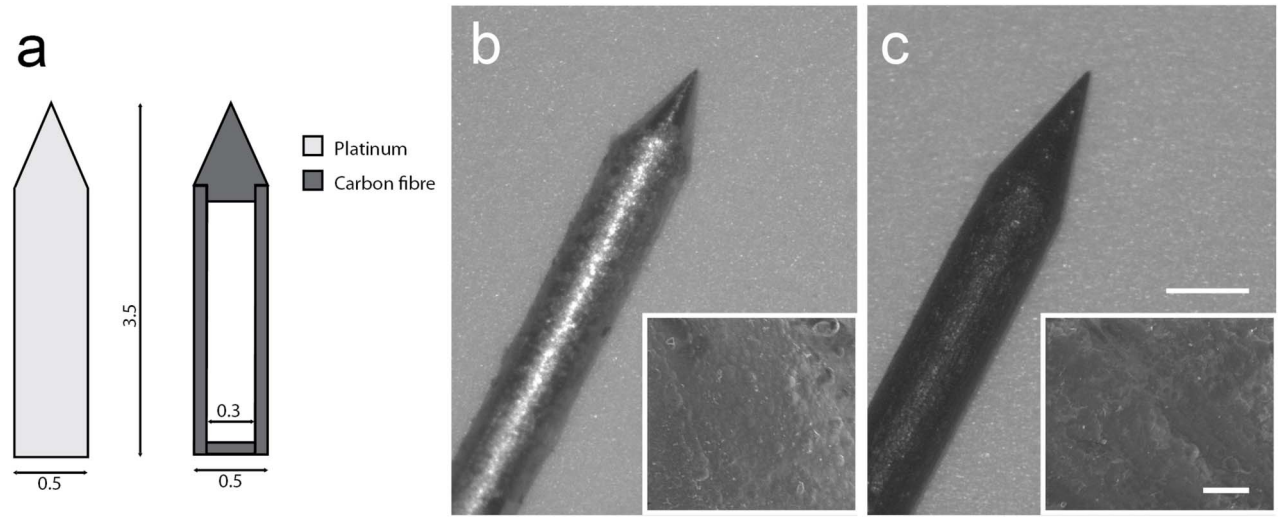

Figure 1 | Visualization of probes used for implantation (a) Schematic overview of the two different types of implant. Images are not to scale; all measurements are in millimetres. (b) Photograph of a high-density probe. The inset is a high magnification scanning electron microscopy image of the surface structure of the parylene C layer. (c) Photograph of a low-density probe. The inset is a high magnification of the surface structure of the parylene C layer. The scale bar in larger image represents 0.5 mm for both (b) and (c), and the scale bar in inset image represents 10 μm for both (b) and (c).

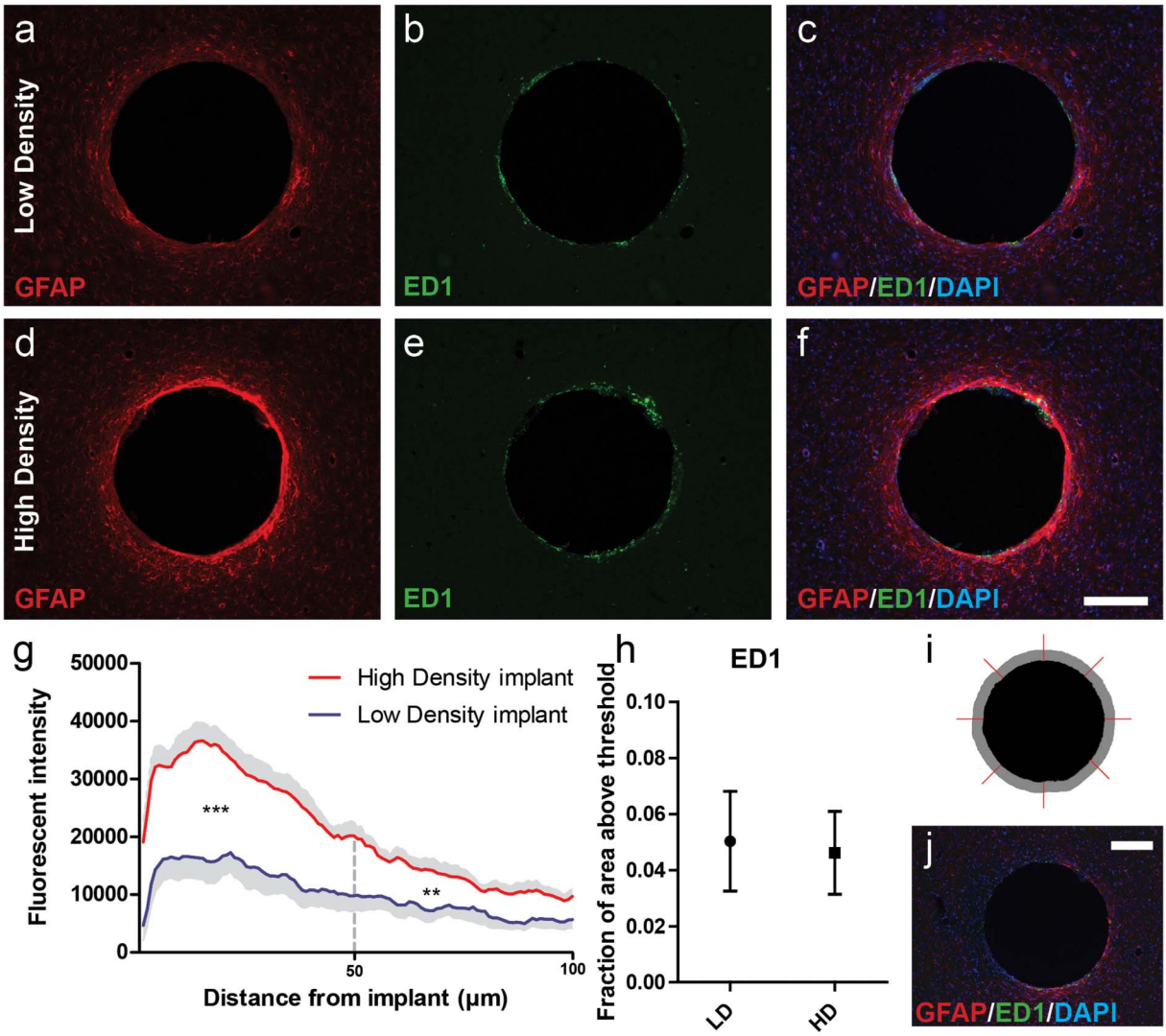

Figure 2 | Low-density probes exhibit smaller tissue reactions (a–c) Representative image of a tissue reaction to low-density implants; GFAP (a), ED1 (b) and merge with DAPI (c), respectively. (d–f) Representative images of tissue reaction to high-density implants; GFAP (d), ED1 (e), and merge with DAPI (f). The scale bar in (f) represents 200 μm for (a–f). (g) Mean intensity profiles for GFAP staining; the grey area signifies the standard error of the mean. Significant differences were seen between area under the curve both in the 0–50 μm ROI ($P = 0.001$) and in the 50–100 μm ROI ($P = 0.0019$). (h) Quantification of ED1 responses; symbol and error bars signify the mean and the SEM. LD, low-density probe; HD, high-density probe. Y-axis is the fraction of area within the ROI above the threshold. There was no significant difference between the ED1 area over the threshold ($P = 0.81$). (i) Illustration of the different quantification methods; the black area is the outline of the hole in (a–c), the red lines are the intensity profile lines used for quantifying GFAP, the grey area is the ROI used for quantifying ED1 and NeuN. (j) Example image of very limited reactions to an LD probe. Note the near complete absence of astrocytes surrounding a part of the probe. We never saw this surrounding the HD probes. The scale bar represents 200 μm.

way, with the exception of density, to eliminate any confounding factors. Both probes were very similar in shape and size, were coated in identical layers of parylene C with a visually identical surface structure (Fig. 4b,c), were made of very stiff materials, and were implanted in identical fashions. With this study design, we believe that we have isolated the effect of the density on the tissue reactions, since it is the only significant difference between the two probes. The parylene C layer negates the effect of the difference in underlying material, and all other parameters are very similar. Thus, any difference found should be largely an effect of the difference in density.

The major findings of the study were that LD probes caused significantly smaller astrocytic scars than did HD probes, and that significantly more microglial cells attached to the explanted HD probes than to the LD probes. This indicates that the density of untethered probes is a significant factor in the development of chronic tissue reactions. Furthermore, this is a clear indication that inertial forces arising due to differences in density between probe and tissue are enough to elicit substantial astrocytic reactions. This provides solid evidence that such forces, and in extension any type of mechanical forces between implant and tissue, play a large role in glial scarring.

The tissue reaction towards neural probes in general, and the astrocytic and microglial reactions in particular, have been extensively studied over the last decade[8,10,12,14–16,20,22–27]. One of the more consistent findings is that untethered rigid probes leave a much smaller scar than do rigid probes that are tethered to the skull[14–16], probably because tethered probes translate movements between the brain and the skull. However, there is still a substantial scar of reactive astrocytes surrounding the untethered probes. Given the present results, the explanation for the observation that untethered probes also left substantial scars could very well be that there are substantial inertial and gravitational forces between tissues and probes because

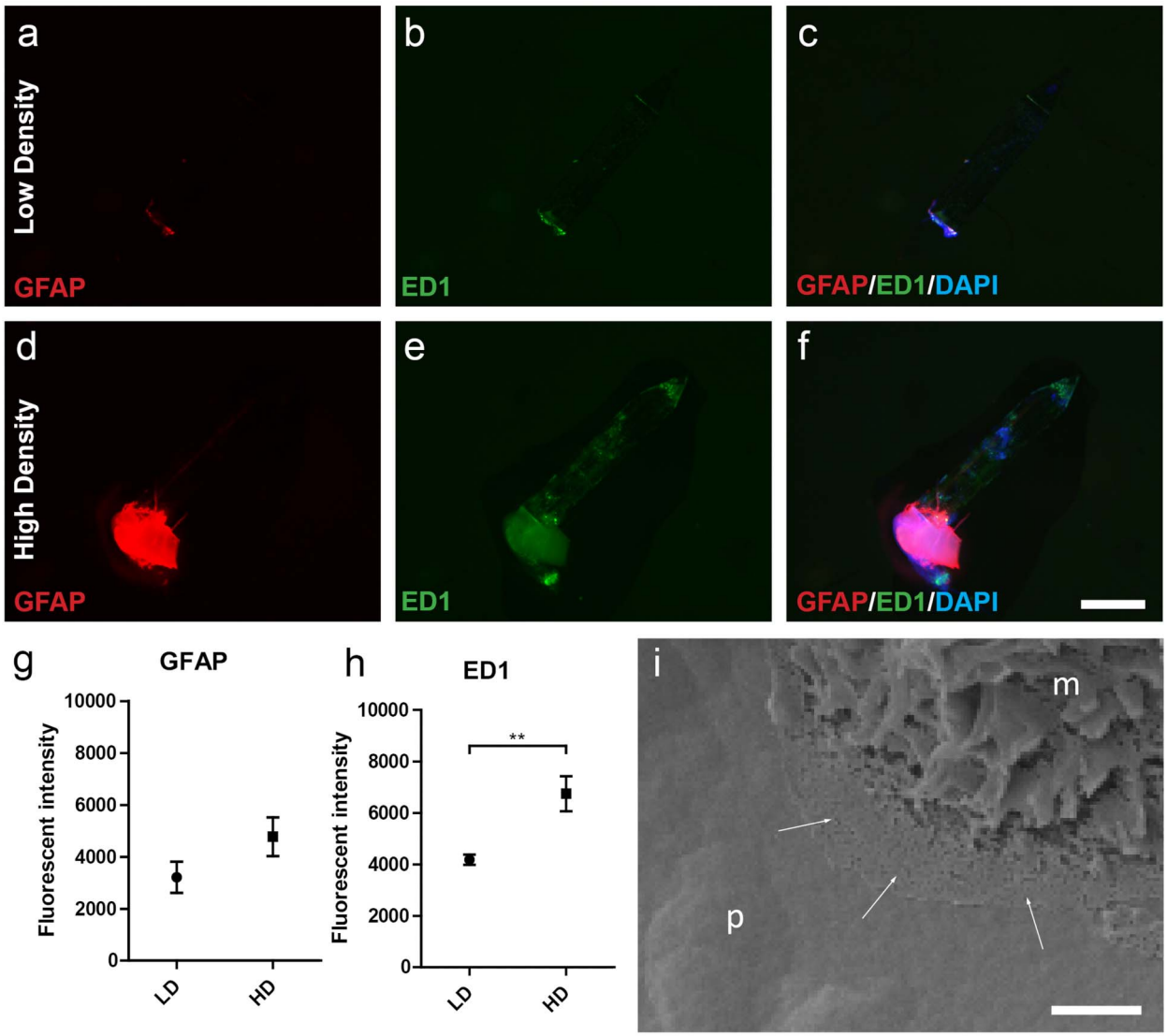

Figure 3 | Explanted high-density probes have more microglial cells attached to them (a–c) Representative image of a low-density implant; GFAP (a), ED1 (b), and merge with DAPI (c). (d–f) Representative image of a high-density implant; GFAP (d), ED1 (e), and merge with DAPI (f). The scale bar in (f) represents 1 mm for (a–f). (g,h) Mean fluorescence intensity of GFAP (g) and ED1 (h) from the ROI of implants. Symbol and error bars signify the mean and SEM, respectively. LD, low-density probe; HD, high-density probe. There was no significant difference between GFAP intensities ($P = 0.16$); however, there was a difference between ED1 intensities ($P = 0.0019$). (i) SEM image of an explanted high-density probe with a cell found attached to it. The parylene C surface is marked with a "p" and a cell, possibly a microglia, is marked with an "m". The white arrows point to the attachment of the cell on the parylene C surface.

of their great difference in density. Electrodes are often made from metals such as stainless steel (density = 8 g/cm^3), tungsten (density = 19.25 g/cm^3), or even platinum (density = 21.45 g/cm^3) and iridium (density = 22.6 g/cm^3), the density of which is much greater than the density of the brain tissue (0.99 g/cm^3)[28]. These differences in density will inevitably lead to inertial forces that arise every time the animal changes direction or velocity. For example, an acceleration of 9.8 m/s^2 (i.e. gravitational acceleration) will result in micro-forces between present HD probe and tissue of roughly 0.5 mN. Thus, we hypothesized that if all these forces approach zero for a probe with a density that is very close to that of the brain, the need for a substantial astrocytic scar would be alleviated, which is exactly what we observed. In fact, several areas surrounding the LD probes (but none surrounding the HD probes) did not have any reactive astrocytes (Fig. 2j), which was never observed in our previous experiments[16,19,20]. Hence, given that the probes used here are very similar apart from with respect to density, we propose that the mechanical forces between probes and neural tissues that arise because of differences in inertial forces every time the animal accelerates or because of difference in gravitational pull on the implants trigger astrocyte reactivity and the development of a glial scar. This is in line with recent findings that the mechanical stimulation of astrocytes renders them reactive, with high expression levels of GFAP[29].

Notably, while a reduction in the inertia forces will result in a reduced need for local anchoring in the tissue to retain a stable position, the finding that a number of LD probes in this study were displaced show that some form of anchoring is still needed. A reduced need for anchoring is beneficial when considering the explantation of probes, especially for human use. If any complications, such as infection or electrode malfunctioning, ensue after implantation of an electrode in a human, it is of utmost importance that the implanted probe can be safely removed. Furthermore, a perfectly floating electrode, without any external forces acting on it, could open up possibilities of studying a particular neuron reliably

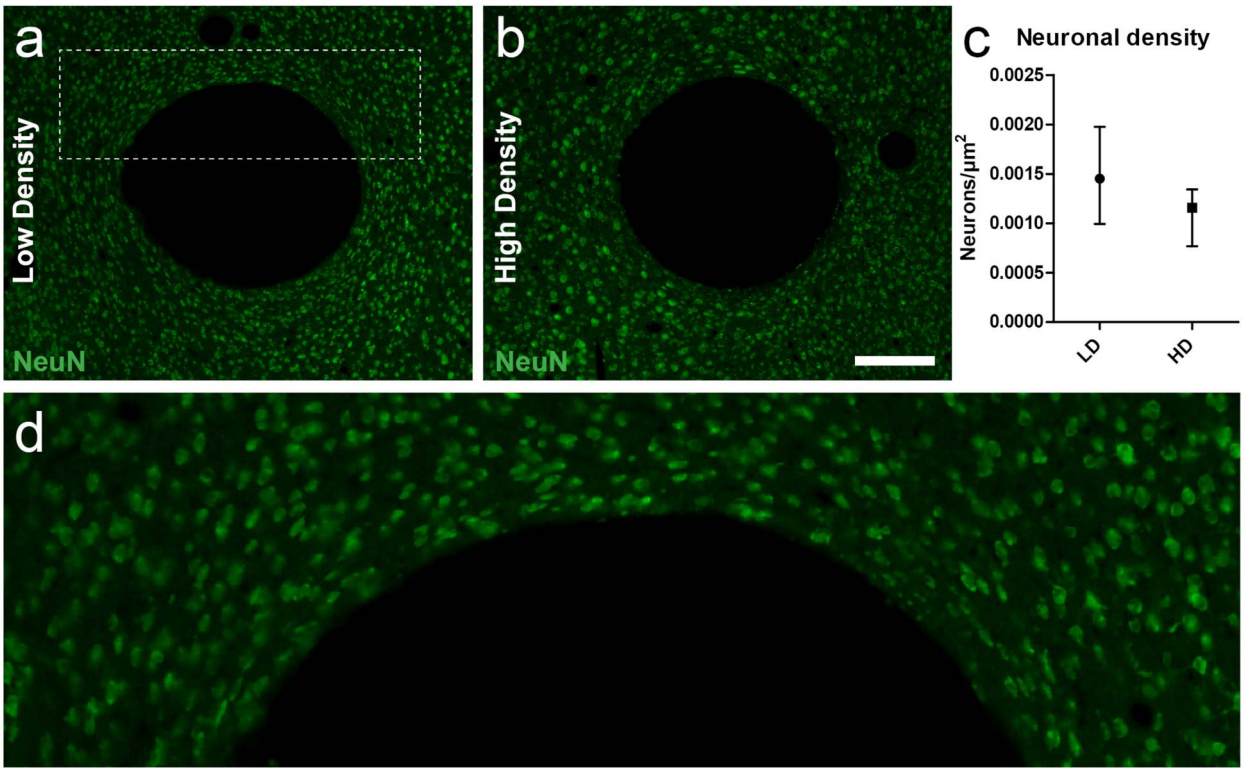

Figure 4 | NeuN staining of neurons in immediate vicinity of probes (a–b) Representative images of NeuN staining in a low-density probe and a high-density probe. The scale bar in (b) represents 200 μm for (a) and (b). (c) Quantification of neuronal densities in the 0–50 μm ROI. Symbol and error bars signify the median and interquartile range, respectively. There was no significant difference between the LD and HD probes ($P = 0.16$). (d) Close-up of the area highlighted in (a). Note the presence of NeuN-positive cells very close to the edge of the wound.

over very long periods of time, or even achieve stable chronic intracellular recording in freely moving animals, something which is not possible with electrodes available today.

To provide a more complete picture of the *in vivo* glial scarring process, we also stained the explanted probes for microglia and astrocytes. These experiments showed that there were practically no GFAP-positive cells along the shanks of either type of probe, whereas there was a significantly greater immunoreactivity for ED1 on the HD probes, indicating that the *in vivo* glial scar contains more microglia surrounding the HD probes even if no such difference is seen in the tissue sections. This also highlights a potential problem inherent to all types of biocompatibility studies in which the probes have to be explanted prior to histological analysis, because rather substantial amounts of microglia, other unknown cells, and to a much smaller extent, astrocytes may be explanted together with the probe and are not accounted for in the analyses of tissue sections[21].

The probes used in this study were larger than the electrodes that are used in current experiments, such as the Michigan probe (with typical shank dimensions of 15×60 μm[30]) or the Utah probe (with a typical shank diameter of less than 90 μm[31]) and the probes used in biocompatibility studies from our laboratory (where diameters of approximately 200 μm is the largest used hitherto[16,19,20]). Despite this, the astrocytic reactions elicited by LD probes are some of the lowest we have seen in long-term studies of neural probes. This is in contrast with the results of other long-term studies performed both by our group and other groups, which showed that larger probes left larger glial scars[16,27]. In light of the results of the current study, and especially the extremely low reactions to the LD probes observed, we would like to propose that such differences are mostly due to differences in inertia forces, and not a direct effect of size. Even if the density of a smaller probe is identical to that of a larger one of the same material, the forces arising from the inertia difference are increased proportionally with the mass of the probes. Thus, the effect of size of the implant on tissue reactions seen in these studies[16,27] might be a foregone conclusion. Hence, the relation between the size and the tissue reactions may be largely abolished if the density of the implanted probe comes close to that of the brain tissue. Further studies are required to reach a definitive conclusion on this issue. It should be pointed out, however, that this may only be true for the chronic scar; the acute damage caused by implantation will always be larger for a larger probe.

The effect of the inertia forces on the astrocytic reaction is not only interesting from a neural interface standpoint; it also constitutes a possible confounding factor for other *in vivo* biocompatibility studies involving neural implants as well as implants in other parts of the body, exemplified by size as discussed above. As such, we believe that density-regulated probes, that is with a density identical to that of the surrounding tissue (0.99 g/cm^3 in the brain[28]), that remain entirely stable in the tissue may be used as a valid platform for testing other aspects of probe design and their true effect on biocompatibility. The results of studies of aspects such as surface structure and material could easily be confounded if the probes were not entirely stable in the tissue, and a completely density-regulated probe is a prerequisite for such stability. The LD probe used in this study is a good step in the right direction and clearly illustrates the effect of density and inertia forces, even if it is not completely density-regulated. The density of this probe was 1.16–1.48 g/cm^3, which is much lower than that of any other probes available (the most lightweight probes in widespread use today are silicon probes, made from silicon, with a density of 2.3 g/cm^3, and some sort of metal with a much higher density), but is still not identical to that of the tissue. It is feasible however, that fully functional electrodes with a density very close to 1 g/cm^3 could be manufactured, for instance using polymer substrates such as PEDOT[32] or carbon fibre[33] instead of metal as conductive material.

It should be kept I mind though, that in order to achieve a tissue friendly neural interface, there are also other parameters to consider. One such factor is the flexibility of the substrate, since a flexible material should be better suited for mitigating any forces acting on the probes and thus might be more suitable as probe materials[2]. It is thus conceivable that a neural interface that combines a tissue matched density and high flexibility will reduce the tissue reactions even further. However, the impact of these design features on long term performance of neural interfaces needs to be carefully evaluated in further studies. In conclusion, the results of our study indicate that the density of a probe strongly impacts the development of the astrocytic scar, as well as the microglial reactions to the probe. This is most likely due to the inertial and gravitational forces elicited by a probe with a higher density than the surrounding tissue, which in turn leads to mechanical stress on the tissue. This implies that the ideal neural implant should have a density of 1 g/cm^3, which would remove most of the glial scar, as well as provide very high stability, potentially allowing long-term recording of single units or even intracellular recordings. Furthermore, we hypothesized that inertial forces can be a confounding factor in many types of biocompatibility studies, which implies that density-regulated implants have the potential of providing a new, valid platform for the testing of biocompatibility properties.

Methods

Implants. Two different types of probes (n = 20 for each probe) were used for implantation: pure platinum needles 500 μm in diameter and 3.5 mm in length (referred to as high-density (HD) probes) and hollow carbon fibre needles that were nearly identical in size and shape to the platinum needles (referred to as low-density (LD) probes) (Fig. 1). To allow a comparison of the tissue reactions to the two probe types, that is not confounded by differences in surface materials, both probes were coated with a 3-μm-thick layer of parylene C, using a Compact Bench Top Coating System (Labtop 3000, Para Tech Coating Inc., CA, US). The parylene coating is formed on the probe surfaces by polymerization of a gas of parylene C monomers. We also examined the surface structure of each probe using a scanning electron microscope (SEM) to ensure that there are minimal differences between the probes (Fig 1b–c). The parylene surfaces of both LD and HD probes were found to be very smooth, with any slightly uneven parts being in the single μm-range. No systematic differences between the surfaces of the two probe types were found. The probes were manufactured in our mechanical workshop. The density of the LD probes was measured by immersing them in a highly concentrated calcium chloride solution, with a density of 1.5 g/cm^3, in which all the probes were floating on the surface of the solution. Then, the solution was diluted until the probe was floating in the middle of the solution, rather than on the surface, but not sinking to the bottom; subsequently, the density of the solution was measured by weighing 1 ml of the solution. Care was taken to avoid air bubbles attaching to the implants or occurring on the surface of the solution. All LD probes had a density between 1.16–1.48 g/cm^3 and the density of the HD probes was very close to that of pure platinum (21.45 g/cm^3).

Ethics, animals, and anaesthesia. All procedures in this study were approved in advance by the Malmö/Lund Animal Ethics Committee on Animal Experiments (permit number M300-10). Implantations were made in female Sprague Dawley rats (n = 20, Taconic, Denmark) weighing 200–250 g. Animals were kept in a 12 h light/dark cycle with access to food and water *ad libitum*. The rats were anaesthetized via intraperitoneal injections of fentanyl (0.3 mg/kg of body weight) and medetomidin hydrochloride (Domitor vet, 0.3 mg/kg of body weight). After surgery, the animals received subcutaneous injections of an antidote to the anaesthesia (Antisedan, atipamezole hydrochloride, 0.5 mg/kg of body weight) as well as Temgesic (buprenorphine, 50 μg/kg of body weight), to reduce postoperative pain.

Surgery. The skin was incised and deflected revealing the area between bregma and lambda. Craniotomies of approximately 1.5 × 1.5 mm were made bilaterally at co-ordinates 3 mm caudal and 3 mm lateral of bregma. The dura mater was incised and deflected. Probes were attached to a micromanipulator using dissolvable gelatine (type B, VWR BDH, Sweden) and implanted at a speed of 10 μm/s to a depth of approximately 3.5 mm, not leaving any part of the probe above the brain surface. The LD probe was implanted in one hemisphere and the HD probe in the other. The gelatine that attached the probes was rinsed with saline after implantation, to release the probes from the micromanipulator with minimal mechanical disturbance[20]. The dura mater was carefully folded back on top of the implants, when possible. The skin was closed using surgical clips or resorbable ethilon sutures (Ethicon, IL, USA). After surgery the animals were returned to the animal house and were not restrained in any way in their cages.

Immunohistochemistry. After 6 weeks, the animals were killed using an overdose of sodium pentobarbital intraperitoneally and perfused transcardially with 0.9% saline solution, followed by 4% formaldehyde in phosphate-buffered saline (PBS). The brains were dissected out and placed in postfix (4% formaldehyde in PBS) overnight, and were then cryoprotected in 25% sucrose in PBS until they no longer floated. The probes were carefully explanted manually using forceps prior to freezing the brains and placed in potassium PBS (KPBS) for further evaluation. A small manual cut was made in the posterior part of the right hemisphere of each brain to be able to identify the hemispheres in individual sections. The brains were cryosectioned horizontally in increments of 30 μm using a sliding knife microtome (Microm, Germany) and placed in KPBS or anti-freeze (30% ethylenglykol, 30% glycerol and 40% PBS) if not analysed immediately. Sections from both hemispheres were stained free-floating together in the same vial, to ensure minimal methodological differences between the two hemispheres. Tissue sections and explanted probes were rinsed in KPBS and incubated overnight in blocking solution (KPBS with 5% normal goat serum (PAA, Austria) and 0.25% Triton X-100 (Fluka/Sigma-Aldrich, Switzerland)), followed by incubation with primary antibodies (rabbit anti-GFAP, 1 : 5000, Dako, Denmark; mouse anti-CD68/ED1, 1 : 250, AbD Serotec, UK; mouse anti-NeuN, 1 : 100, Millipore, USA) diluted in blocking solution. Thereafter, sections were incubated for 2 h in secondary antibodies (goat anti-rabbit Alexa Fluor 594 and goat anti-mouse Alexa Fluor 488, 1 : 500, Invitrogen, USA) and 4′,6-diamidino-2-phenylindole (DAPI, 1 : 1000, Invitrogen, USA) diluted in blocking solution. Sections were mounted onto chrome alum-coated glass slides and covered with cover-slips using PVA/DABCO (Fluka/Sigma-Aldrich, Switzerland).

Image acquisition and analysis. All immunofluorescence images were acquired using a DS-2MV digital camera (Nikon, Japan) mounted on a Nikon eclipse 80i microscope (Nikon, Japan) with a 10× objective for sections and a 2× objective for images of probes. Identical filters, gains, and exposure times were used for all images of a certain marker. Analysis of images was made using the NIS-elements 3.1 software (Nikon, Japan). Images were taken from the same section for both sides when possible, from an approximate cortical depth of 1 mm. Different quantification methods were used for the different markers. For GFAP staining, eight 100 μm intensity profile lines were set radiating evenly from the edge of the wound (Fig. 2i). The profile lines were placed blindly leaving only the rim of the wound visible. The background for each image was subtracted from the profile. Area under curve was calculated for 0–50 μm and 50–100 μm for the mean profile of each image. For ED1 staining, the quantification method used in our previous studies was used[16,19,20]. This was because the ED1 staining was too sparse to allow the use of the same quantification method applied to the GFAP staining, and was too diffuse to allow counting cells. A region of interest (ROI) was set at a distance of 0–50 μm from the rim of the wound (Fig. 2i), as this is where practically all of the ED1 cells are found. Intensity thresholds were set at five times the background intensity and the area with intensity above threshold in the ROI was calculated. Regarding NeuN staining, the same ROI was used (0–50 μm); the number of positively labelled cells was counted manually and the number of neurons per μm^2 was calculated.

The explanted probes were analysed by placing a ROI along the probe at 0.5–1.5 mm from the top of the probe. This was done to analyse approximately the same region as that from which the sections were chosen. The mean intensity of ED1 and GFAP staining was measured in the ROI.

SEM images of probes prior to implantation were taken using a SU1510 microscope (Hitachi, Japan). Explanted probes were dehydrated in rising concentrations of alcohol prior to critical point drying (Valtec CPD030, Leica Microsystems, Sweden) and sputter-coated using Gold-Palladium (Polaron SC7640, VG Microtech, UK). Images were then taken using a SU3500 microscope (Hitachi, Japan).

Excluded animals and statistics. Out of the 20 animals that were implanted, two were killed prior to the end-point because of the premature loosening of their surgical clips, and four animals were excluded from the study because of both probes being found displaced, i.e. on the surface of the skull or deep inside the brain. Of the remaining 14 animals, nine had both probes remaining in place at the time of dissection; thus, both probes were analysed. In three animals, the LD probe was found on top of the skull: only the HD probe was analysed in the animals. In two animals, the HD probes had sunk through the brain and were found in the corpus callosum or hippocampus: only the LD probe was analysed in these animals. This left 11 animals from which the LD probes were analysed and 12 animals from which the HD probes were analysed.

A non-parametric statistical test, the Mann–Whitney test, was used in this study. Comparisons were made between the LD and HD probes for each staining in each respective ROI. $P < 0.05$ was considered significant and is marked by *; a $P < 0.01$ is marked by **; and $P < 0.001$ is marked by ***.

1. Kipke, D. R. *et al.* Advanced neurotechnologies for chronic neural interfaces: new horizons and clinical opportunities. *J Neurosci* **28**, 11830–11838 (2008).
2. Schouenborg, J. Biocompatible multichannel electrodes for long-term neurophysiological studies and clinical therapy–novel concepts and design. *Prog Brain Res* **194**, 61–70, doi:10.1016/B978-0-444-53815-4.00017-0 (2011).
3. Polikov, V. S., Tresco, P. A. & Reichert, W. M. Response of brain tissue to chronically implanted neural electrodes. *J Neurosci Methods* **148**, 1–18 (2005).
4. Rousche, P. J. & Normann, R. A. Chronic recording capability of the Utah Intracortical Electrode Array in cat sensory cortex. *J Neurosci Methods* **82**, 1–15 (1998).

5. Williams, J. C., Rennaker, R. L. & Kipke, D. R. Long-term neural recording characteristics of wire microelectrode arrays implanted in cerebral cortex. *Brain Res Brain Res Protoc* **4**, 303–313 (1999).
6. Marin, C. & Fernandez, E. Biocompatibility of intracortical microelectrodes: current status and future prospects. *Front Neuroeng* **3**, 8, doi:10.3389/fneng.2010.00008 (2010).
7. McConnell, G. C., Butera, R. J. & Bellamkonda, R. V. Bioimpedance modeling to monitor astrocytic response to chronically implanted electrodes. *J Neural Eng* **6**, 055005 (2009).
8. Szarowski, D. H. *et al.* Brain responses to micro-machined silicon devices. *Brain Res* **983**, 23–35 (2003).
9. Williams, J. C., Hippensteel, J. A., Dilgen, J., Shain, W. & Kipke, D. R. Complex impedance spectroscopy for monitoring tissue responses to inserted neural implants. *Journal of Neural Engineering* **4**, 410–423, doi:10.1088/1741-2560/4/4/007 (2007).
10. Biran, R., Martin, D. C. & Tresco, P. A. Neuronal cell loss accompanies the brain tissue response to chronically implanted silicon microelectrode arrays. *Exp Neurol* **195**, 115–126 (2005).
11. Edell, D. J., Toi, V. V., McNeil, V. M. & Clark, L. D. Factors influencing the biocompatibility of insertable silicon microshafts in cerebral cortex. *IEEE transactions on bio-medical engineering* **39**, 635–643, doi:10.1109/10.141202 (1992).
12. McConnell, G. C. *et al.* Implanted neural electrodes cause chronic, local inflammation that is correlated with local neurodegeneration. *J Neural Eng* **6**, 56003 (2009).
13. Gilletti, A. & Muthuswamy, J. Brain micromotion around implants in the rodent somatosensory cortex. *Journal of Neural Engineering* **3**, 189–195, doi:10.1088/1741-2560/3/3/001 (2006).
14. Biran, R., Martin, D. C. & Tresco, P. A. The brain tissue response to implanted silicon microelectrode arrays is increased when the device is tethered to the skull. *J Biomed Mater Res A* **82**, 169–178 (2007).
15. Kim, Y. T., Hitchcock, R. W., Bridge, M. J. & Tresco, P. A. Chronic response of adult rat brain tissue to implants anchored to the skull. *Biomaterials* **25**, 2229–2237 (2004).
16. Thelin, J. *et al.* Implant size and fixation mode strongly influence tissue reactions in the CNS. *PLoS One* **6**, e16267, doi:10.1371/journal.pone.0016267 (2011).
17. Freire, M. A. *et al.* Comprehensive analysis of tissue preservation and recording quality from chronic multielectrode implants. *PLoS One* **6**, e27554, doi:10.1371/journal.pone.0027554 (2011).
18. Williams, D. F. *The Williams dictionary of biomaterials.* (Liverpool University Press, 1999).
19. Lind, G., Gallentoft, L., Danielsen, N., Schouenborg, J. & Pettersson, L. M. Multiple implants do not aggravate the tissue reaction in rat brain. *PLoS One* **7**, e47509, doi:10.1371/journal.pone.0047509 (2012).
20. Lind, G., Linsmeier, C. E., Thelin, J. & Schouenborg, J. Gelatine-embedded electrodes–a novel biocompatible vehicle allowing implantation of highly flexible microelectrodes. *Journal of Neural Engineering* **7**, 046005, doi:10.1088/1741-2560/7/4/046005 (2010).
21. Turner, J. N. *et al.* Cerebral Astrocyte Response to Micromachined Silicon Implants. *Experimental Neurology* **156**, 33–49 (1999).
22. Eriksson Linsmeier, C. *et al.* Nanowire biocompatibility in the brain–looking for a needle in a 3D stack. *Nano Lett* **9**, 4184–4190 (2009).
23. Grill, W. M., Norman, S. E. & Bellamkonda, R. V. Implanted neural interfaces: biochallenges and engineered solutions. *Annu Rev Biomed Eng* **11**, 1–24 (2009).
24. He, W., McConnell, G. C. & Bellamkonda, R. V. *Journal of Neural Engineering* Nanoscale laminin coating modulates cortical scarring response around implanted silicon microelectrode arrays. **3**, 316–326, doi:10.1088/1741-2560/3/4/009 (2006).
25. McConnell, G. C., Schneider, T. M., Owens, D. J. & Bellamkonda, R. V. Extraction force and cortical tissue reaction of silicon microelectrode arrays implanted in the rat brain. *IEEE transactions on bio-medical engineering* **54**, 1097–1107, doi:10.1109/TBME.2007.895373 (2007).
26. Seymour, J. P. & Kipke, D. R. Neural probe design for reduced tissue encapsulation in CNS. *Biomaterials* **28**, 3594–3607, doi:10.1016/j.biomaterials.2007.03.024 (2007).
27. Stice, P., Gilletti, A., Panitch, A. & Muthuswamy, J. Thin microelectrodes reduce GFAP expression in the implant site in rodent somatosensory cortex. *Journal of Neural Engineering* **4**, 42–53 (2007).
28. Beckmann, F. *et al.* Three-Dimensional Imaging of Nerve Tissue by X-Ray Phase-Contrast Microtomography. *Biophysical Journal* **76**, 98–102, doi:http://dx.doi.org/10.1016/S0006-3495(99)77181-X (1999).
29. Wanner, I. B. An in vitro trauma model to study rodent and human astrocyte reactivity. *Methods Mol Biol* **814**, 189–219, doi:10.1007/978-1-61779-452-0_14 (2012).
30. Vetter, R. J., Williams, J. C., Hetke, J. F., Nunamaker, E. A. & Kipke, D. R. Chronic neural recording using silicon-substrate microelectrode arrays implanted in cerebral cortex. *IEEE transactions on bio-medical engineering* **51**, 896–904, doi:10.1109/TBME.2004.826680 (2004).
31. Campbell, P. K., Jones, K. E., Huber, R. J., Horch, K. W. & Normann, R. A. A silicon-based, three-dimensional neural interface: manufacturing processes for an intracortical electrode array. *IEEE Trans Biomed Eng* **38**, 758–768 (1991).
32. Ludwig, K. A., Uram, J. D., Yang, J., Martin, D. C. & Kipke, D. R. Chronic neural recordings using silicon microelectrode arrays electrochemically deposited with a poly(3,4-ethylenedioxythiophene) (PEDOT) film. *Journal of Neural Engineering* **3**, 59–70, doi:10.1088/1741-2560/3/1/007 (2006).
33. Kozai, T. D. *et al.* Ultrasmall implantable composite microelectrodes with bioactive surfaces for chronic neural interfaces. *Nat Mater* **11**, 1065–1073, doi:10.1038/nmat3468 (2012).

Acknowledgements

This study was financed by a Linnaeus grant (Project number 600012701) from the Swedish research council and the Medical Faculty at Lund University as well as a grant from the Knut and Alice Wallenberg foundation (KAW 2004.0119). The authors would like to thank Suzanne Rosander-Jönsson and Lars-Åke Clemendz for invaluable technical support and Johan Agorelius and Fredrik Johansson for help with electron microscopy.

Author contributions

G.L., C.E.L. and J.S. designed the experiments. G.L. performed the experiments and the analyses. G.L., C.E.L. and J.S. wrote the manuscripts.

Additional information

Competing financial interests: G.L. and J.S. are co-authors of a patent application (PCT: WO 2012/025596) regarding a density regulated electrode. C.E.L. has no competing financial interests.

How to cite this article: Lind, G., Linsmeier, C.E. & Schouenborg, J. The density difference between tissue and neural probes is a key factor for glial scarring. *Sci. Rep.* **3**, 2942; DOI:10.1038/srep02942 (2013).